PCCP

RSC Publishing

PAPER

View Article Online
View Journal | View Issue

Cite this: *Phys. Chem. Chem. Phys.*, 2013, **15**, 20496

Oxidation of gas-phase hydrated protonated/deprotonated cysteine: how many water ligands are sufficient to approach solution-phase photooxidation chemistry?

Fangwei Liu, Rifat Emre, Wenchao Lu and Jianbo Liu*

Received 4th September 2013,
Accepted 16th October 2013

DOI: 10.1039/c3cp53736f

www.rsc.org/pccp

We present a study on the reactions of singlet oxygen $O_2[a^1\Delta_g]$ with hydrated protonated and deprotonated cysteine (Cys) in the gas phase, including measurements of the effects of collision energy (E_{col}) and hydration number on reaction cross sections over a center-of-mass E_{col} range from 0.05 to 1.0 eV. The aim is to probe how successive addition of water molecules changes the oxidation chemistry of Cys in the gas phase. Hydrated clusters, generated by electrospray ionization, have structures of $HSCH_2CH(NH_3^+)CO_2H(H_2O)_{1,2}$ and $HSCH_2CH(NH_2)CO_2^-(H_2O)_{1,2}$ for protonated and deprotonated forms, respectively. In contrast to $^1O_2$ reactions with dehydrated protonated/deprotonated Cys of which hydroperoxide products all decomposed, reactions with hydrated protonated/deprotonated Cys yielded stable hydroperoxide products, analogous to photooxidation reaction of Cys in solution. We investigated the number of water ligands necessary to produce a stable hydroperoxide, and found that a single water molecule suffices—that is, to relax nascent, energized hydroperoxide in the hydrated cluster by elimination of water. Hydrated protonated Cys shows higher reaction efficiency than the hydrated deprotonated one, particularly with the addition of the second water ligand. Reactions of hydrated protonated/deprotonated Cys are suppressed by E_{col}, becoming negligible at $E_{col} \geq 0.5$ eV. Density functional theory calculations were used to locate reaction coordinates for these systems. Quasi-classical, direct dynamics trajectory simulations were performed for $HSCH_2CH(NH_3^+)CO_2H(H_2O)$ + $^1O_2$ at the B3LYP/4-31G(d) level of theory. Analysis of trajectories highlights the importance of complex mediation in the early stages of the reaction, and illustrates that water can catalyze proton transfer within the hydrated complex.

I. Introduction

Singlet molecular oxygen (O_2, $a^1\Delta_g$) is produced in biological systems *via* various paths,[1] and oxidation of amino acids by $^1O_2$ is an important process associated with biological aging, diseases,[2] and photodynamic therapy for cancer treatment.[3] Because of these biological as well as photochemical implications in the atmosphere,[4] there has been considerable interest in studying $^1O_2$-induced amino acid oxidation mechanisms. Most of these experiments were carried out in solution using photosensitization methods[5] (referred to as "photooxidation"). In photooxidation experiments, $^1O_2$ was generated by sensitizers upon exposure to ultraviolet/visible light,[6] *i.e.*, sensitizer $\xrightarrow{h\upsilon}$ sensitizer*, followed by sensitizer* $+^3O_2$ $\xrightarrow{\text{energy transfer}}$ sensitizer $+^1O_2$. Photooxidation of amino acids often shows complex features with multiple pathways and products depending on pH, oxygen concentration, solvent composition, type of sensitizers, buffer ions, *etc.* These are partly due to the fact that type I (free radical-mediated) and type II ($^1O_2$-mediated) mechanisms might co-exist in photooxidation; as a consequence, other reactive oxygen species besides $^1O_2$ may contribute to oxidation reactions. These factors complicate reaction systems, requiring multiple sets of control experiments in order to obtain a good understanding of oxidation mechanisms in solution.

To avoid the complexities/interferences arising from solution-phase experiments and simplify the interpretation of the oxidation mechanisms of amino acids, we have looked at the reactions of $^1O_2$ with protonated and deprotonated amino acids in the gas phase[7–11] using electrospray-ionization (ESI)[12,13] mass spectrometry and guided-ion-beam scattering methods.[14] One advantage of investigating biomolecules in the gas phase is that it allows one to observe single molecules separated from bulk solution environments. In this way, intrinsic reactivity of molecules

Department of Chemistry and Biochemistry, Queens College and the Graduate Center of the City University of New York, 65-30 Kissena Blvd., Queens, New York 11367, USA. E-mail: jianbo.liu@qc.cuny.edu

can be distinguished from solvent effects. By combining gas-phase experiments, statistical modeling and molecular dynamics simulations, we were able to unravel oxidation mechanisms and dynamics of various gas-phase "bare" amino acid ions, including protonated tyrosine,[7] methionine,[8] cysteine and tryptophan,[9] and deprotonated tyrosine, tryptophan[10] and cysteine.[11]

However, an obvious question for gas-phase experiments of protonated/deprotonated amino acids with $^1O_2$ is how to make these reactions closely resemble photooxidation reactions in biological systems where amino acids are solvated. Because amino acid ions are able to form hydrogen bonds with water molecules, it is often difficult to distinguish the effects caused by the intrinsic properties of amino acid ions from those caused by their interactions with water.[15] In theory, this question might be addressed by a comparison of gas- and solution-phase reaction products. In practice, such comparison may become difficult considering the technical limitations of solution-phase photooxidation experiments. In addition, a simple comparison of gas- and solution-phase reactions may not be able to provide information about the effects of individual water molecules on amino acid oxidation.

Let us take the reaction of cysteine (Cys) with $^1O_2$ as an example.[16–22] Cys is one of the most susceptible residues towards oxidative damage by $^1O_2$ in proteins.[1,2,23] Photooxidation of Cys initially forms a persulfoxide intermediate (note that persulfoxide is a well-known key intermediate in reactions of $^1O_2$ with organic sulfides,[24] albeit less common in thiol + $^1O_2$ reactions). Ultimate oxidation products of Cys include cystine, RSO_2H, and other species that remain to be elucidated. Photooxidation of Cys shows pH dependence, *i.e.*, in acidic solution, Cys is converted to RSO_2H; while in neutral or alkaline media, oxidation is completed by a dark reaction, resulting in cystine rather than RSO_2H.[25]

We have investigated the reactions of $^1O_2$ with protonated and deprotonated Cys, respectively, in the gas phase.[9,11] For protonated $CysH^+$, the product channel corresponds to C^{α}–C^{β} bond rupture of a hydroperoxide intermediate $Cys\text{-}SOOH^+$ accompanied by intra-molecular H atom transfer, and subsequent dissociation to $H_2NCHCO_2H^+$, CH_3SH and $^3O_2$. Deprotonated $[Cys\text{-}H]^-$ has a carboxylate structure $HSCH_2CH(NH_2)CO_2^-$, and three product channels were observed for its reaction with $^1O_2$. Dissociation of $HSCH_2CH(NH_2)CO_2^-$ to $NH_2CH_2CO_2^-$ and CH_2S accompanied by quenching of $^1O_2$ has the largest cross section. Two minor channels correspond to the formation of $HSCH_2C(NH)CO_2^-$ + H_2O_2 and $OSCH_2CH(NH_2)CO_2^-$ + $^{\bullet}OH$, respectively. Although oxidation of both protonated and deprotonated Cys yields persulfoxide and hydroperoxide intermediates, none of these was detected in product ion mass spectra. Therefore, oxidation of Cys in the gas phase appears to somewhat deviate from what happens in aqueous solution.

To solve this puzzle, in the present paper we report a study on the effects of hydration on oxidation of protonated and deprotonated Cys (as a function of the number of water molecules absorbed). The approach we utilized is to hydrate $CysH^+$ or $[Cys\text{-}H]^-$ by adding water molecules stepwise, and study the reactions of resulting gas-phase hydrated clusters. This approach provides detailed information on the reactivity of solvated Cys ions, without interference arising from the presence of bulk water.[26] In the following sections, we will describe a guided-ion-beam study together with theoretical simulations of the reactions of $^1O_2$ with gaseous hydrated $CysH^+(H_2O)_n$ and $[Cys\text{-}H]^-(H_2O)_n$ (n = 1–2). As we will show, in contrast to that of $CysH^+$ and $[Cys\text{-}H]^-$, oxidation of $CysH^+(H_2O)_{1,2}$ and $[Cys\text{-}H]^-(H_2O)_{1,2}$ results in stable peroxide products, similar to solution-phase photooxidation reactions.

II. Experimental and computational details

2.1 Experimental procedures

The experiment was carried out using a home-made guided-ion-beam tandem mass spectrometer that has been described in previous publications.[7–11,27,28] Only a brief description is given here, emphasizing key operating parameters. For this experiment, both mass filters were operated at 2.1 MHz with a m/z range of 1–500. A sample solution of $CysH^+$ was prepared in HPLC grade methanol–water (1 : 2 vol. ratio) containing 0.5 mM L-cysteine hydrochloride (≥ 99.0%, Fluka), and that of $[Cys\text{-}H]^-$ was prepared in methanol–water (4 : 1) containing a mixture of 0.5 mM L-cysteine (100.1% by titration, EMD Chemicals) and sodium hydroxide (reagent grade, Fisher). The sample solution was sprayed into an ambient atmosphere through an electrospray needle at a flow rate of 0.03–0.04 mL h^{-1}. The electrospray needle was biased at 2000 to 2500 V and −2000 to −2200 V for producing positively and negatively charged species, respectively. Charged droplets entered an ion source chamber through a desolvation capillary. The capillary was held at 90 to 120 V for positive ions and −90 to −100 V for negative ions. Liquid droplets underwent desolvation as they passed through the heated capillary, converting to gas-phase ions in the source chamber. Under mild heating conditions, not all of the solvent was removed, resulting in hydrated ions.[29] In the experiment, the capillary was heated to 130–160 °C for generating monohydrated ions and 110–130 °C for dihydrated ions.

A skimmer with an orifice of 0.99 mm is located 3 mm from the capillary end, separating the source chamber and a radio-frequency (rf) hexapole ion guide. The skimmer was biased at 15 to 20 V for positive ions and −20 V for negative ions. Ions emerging from the skimmer were transported into the hexapole ion guide at a pressure of 20 mTorr and underwent collisional cooling and focusing.[30,31] As characterized by a collision-induced dissociation (CID) experiment,[7] internal energy of primary ions could be described by a Maxwell–Boltzmann distribution at ~310 K. Ions subsequently passed into a quadrupole mass filter for selection of reactant ions. Reactant ions were collected and focused into an octopole ion guide. The octopole passes through a scattering cell containing neutral reactant gas. The cell pressure was measured by a Baratron capacitance manometer (MKS 690 head and 670 signal conditioner). The ion guide minimizes loss of the reactant and product ions resulting from scattering. After passing through the scattering cell, unreacted ions and product ions drifted to the end of the octopole, mass analyzed by a second quadrupole mass filter, and counted.

Initial kinetic energy distribution of the reactant ion beam was determined using a retarding potential analysis,[32] *i.e.*, measuring the intensity of the ion beam while scanning the DC bias voltage applied to the octopole. The DC bias voltage allowed control of the kinetic energy (E_{Lab}) of reactant ions in the laboratory frame. E_{Lab} was converted into the collision energy (E_{col}) between the reactant ion and $^1O_2$ in the center-of-mass frame using $E_{col} = E_{Lab} \times m_{neutral}/(m_{ion} + m_{neutral})$, where $m_{neutral}$ and m_{ion} are the masses of $^1O_2$ and the reactant ion, respectively. The intensity of the reactant ion beam was 2×10^5 counts per second and constant within 10%. The initial kinetic energy of the ion beam was 0.9 to 1.0 eV, and the energy spread was ~0.6 eV which corresponds to an energy spread of ~0.1 eV in the center-of-mass frame for the collisions of $CysH^+(H_2O)_{1,2}/[Cys\text{-}H]^-(H_2O)_{1,2}$ with $^1O_2$. Reaction cross sections were calculated from the ratio of product and reactant ion intensities (under single ion-molecule collision conditions), the calibrated $^1O_2$ pressure, and the effective length of the scattering cell.[33]

$^1O_2$ was generated by the reaction of $H_2O_2 + Cl_2 + 2KOH \rightarrow O_2(X^3\Sigma_g^-$ and $a^1\Delta_g) + 2KCl + 2H_2O$. We adopted this technique from Viggiano's group[34] with some modifications.[8,9] Briefly, 20 mL of 35 wt% H_2O_2 (Acros Organics) was mixed with 13 mL of 8 M KOH (>85%, Fisher) solution in a sparger that was immersed in a cold bath maintained at −19 °C, and the resulting solution was degassed. A continuous flow of He (research grade, T. W. Smith) was then introduced to the slushy H_2O_2–KOH mixture at a flow rate of 50 sccm to prevent freezing of the mixture. Finally, Cl_2 (≥99.5%, Sigma-Aldrich), at a flow rate of 2–3 sccm, was mixed with He in a gas proportioner and bubbled through the H_2O_2–KOH solution. Cl_2 completely reacted with H_2O_2 to form ground-state and excited O_2.[35] The resulting gas mixture passed through a cold trap kept at −70 °C to remove water vapor. Only $^3O_2$, $O_2(a^1\Delta_g)$ and He remained in the downstream gas.

Before leaking into the scattering cell, the gases flowed through an emission cell for detection of $^1O_2$ emission ($a^1\Delta_g \rightarrow X^3\Sigma_g^-$, ν = 0–0) at 1270 nm.[36] The emission cell was continuously pumped through a pressure control valve up to 15 Torr, so as to reduce the residence time and hence the wall quenching of $^1O_2$ inside the cold trap, tubing and emission cell. Emission from the cell was collected by a plano-convex lens, and passed through an optical chopper (SRS model SR540) and a 0.5 nm bandwidth interference filter centered at 1270 nm. Chopped emission was focused into a thermoelectrically cooled InGaAs detector (Newport 71887 detector and 77055 TE-cooler controller), and the signal was processed by a lock-in amplifier (SRS model SR830). To determine the absolute $^1O_2$ concentration, the detection system was calibrated using the known reaction rate for $HS^- + {}^1O_2 \rightarrow SO^- + OH$.[10] $^1O_2$ pressure in the scattering cell is the product of the total gas pressure in the scattering cell, the percentage of Cl_2 in the Cl_2/He flow, and the $^1O_2$ concentration (~10%) in the oxygen product.

Collision cross section ($\sigma_{collision}$), taken as the greater of ion-induced dipole capture cross section ($\sigma_{capture}$)[37] and hard-sphere collision cross section ($\sigma_{hard\text{-}sphere}$), is 73–95 Å^2 for $CysH^+(H_2O)/[Cys\text{-}H]^-(H_2O) + O_2$, and 82–95 Å^2 for $CysH^+(H_2O)_2/[Cys\text{-}H]^-(H_2O)_2 + O_2$ in the E_{col} range of 0.05–1.0 eV. $\sigma_{hard\text{-}sphere}$ was estimated from the orientation-averaged contact radii of reactant ions and O_2, and exceeds $\sigma_{capture}$ at $E_{col} \geq 0.1$ eV. The pressure of O_2/He in the scattering cell was maintained at 0.25 mTorr, which contained 5% of O_2 (including $^3O_2$ and $^1O_2$). This pressure was chosen to provide reasonable intensities of product ions, while keeping multiple-collision effects to a minimum level. At this pressure, the probability of $CysH^+(H_2O)_{1,2}/[Cys\text{-}H]^-(H_2O)_{1,2}$ undergoing a single-collision with O_2 is <2%, and that of double collisions is <0.1%. Note that reactant ions also collided with He, with a single-collision probability of 16–20%, and a double-collision probability of 3–7%. However, the heavy ion–light neutral combination makes these collisions insignificant compared to those with O_2.

Because the signals we measured are small, it is important to minimize systematic variations in experimental conditions that might be caused by drifting potentials, changes in ion beam intensities and $^1O_2$ yield, *etc.* The concentration of $^1O_2$ was monitored continuously during the experiment, and the concentration variation (controlled to be within 20%) was corrected for while calculating reaction cross sections. The entire experiment was repeated several times and each time we cycled through different E_{col} values. The results presented are averages of several complete datasets. Based on the reproducibility of the cross section measurements taken over a two-month period, we estimate that the relative error is <20%. To check the reactivity of $CysH^+(H_2O)_{1-2}$ or $[Cys\text{-}H]^-(H_2O)_{1-2}$ toward $^3O_2$ and He, control experiments were performed under the same conditions except that Cl_2 was replaced by oxygen gas at the same flow rate.

2.2 Computational methods

To interpret reaction coordinates, density functional theory (DFT) electronic structure calculations were performed at the B3LYP level of theory with various basis sets including 6-31+G(d), 6-311++G(d,p) and aug-cc-pVQZ, using Gaussian 09.[38] Geometries were optimized by calculating force constants at every step. All of the transition states (TSs) found were verified to be first-order saddle points, and the vibrational mode with an imaginary frequency corresponds to the associated reaction pathway. Zero-point energies (ZPEs) were scaled by a factor of 0.981[39] in calculating energetics. The molecular structures of reactants, complexes, TSs and products are available on request to the corresponding author.

Quasi-classical, direct dynamics trajectory simulations were used to identify important steps along the reaction coordinate for $CysH^+(H_2O) + {}^1O_2$. Direct dynamics simulations combine electronic structure theory and molecular dynamics directly by solving time-independent Schrödinger equation at each integration step, so that trajectories are calculated on the fly without the need for an analytical potential energy surface.[40] In our simulations, VENUS99[41] was used to set up initial conditions, and the Hessian-based predictor-corrector algorithm[42] available in Gaussian 09 was used to propagate each trajectory with the Hessian matrix updated every five steps. From an analysis of the computer time required to calculate a trajectory at different levels of theory and the overall level of agreement of these different levels with experimental and/or high level benchmark results, the B3LYP/4-31G(d) level was chosen for trajectory simulations.

Trajectory integration was performed with a step size of 0.25 amu$^{1/2}$Bohr (corresponding to a step size of $\sim$0.6 fs in trajectory time), which conserved total energy to better than 10^{-4} Hartree. The SCF = XQC option was adopted during trajectory integration so that a quadratically convergent SCF method[38,43] was used in case the usual, but much faster, first-order SCF method failed to converge within the allotted number of cycles.

The purpose of our trajectory simulations is to probe the gross features of the collisions between $CysH^+(H_2O)$ and $^1O_2$. Particularly, simulations were used to help discover reaction mechanisms. Thus all trajectories were calculated at an impact parameter b of 0.1 Å, rather than sampling the b distribution. Batches of trajectories were calculated at E_{col} of 0.1 and 0.2 eV, respectively. Initial conditions of the reactants were chosen to mimic our experiment. Because $CysH^+(H_2O)$ ions were thermalized in the experiment, their initial vibrational and rotational energies in trajectories were sampled from Boltzmann distributions at 300 K. Similarly, 300 K was used for simulating rotational and vibrational energy distributions of $^1O_2$. Quasi-classical initial vibrational state was simulated by giving each reactant atom displacement from equilibrium and momentum appropriate to the initial rovibrational state, with random phases for different modes. Both $CysH^+(H_2O)$ and $^1O_2$ have ZPEs in all vibrational modes. Randomly oriented $CysH^+(H_2O)$ and $^1O_2$ were given relative velocities corresponding to the simulated E_{col}. All trajectories started with a center-of-mass reactant separation of 8.0 Å, and were terminated after 5000 steps or when the product separation exceeded 8.0 Å. Trajectories were calculated on an Intel core i7 6-core (3.2 GHz)-based Linux workstation cluster, and the actual computer processing time for a trajectory ranged from 200 to 350 CPU hours. gOpenMol[44] was used for trajectory visualization.

III. Results and discussion

3.1 Structures of $CysH^+(H_2O)_{1,2}$ and $[Cys\text{-}H]^-(H_2O)_{1,2}$

In our previous study of $CysH^+ + {}^1O_2$ and $[Cys\text{-}H]^- + {}^1O_2$, we have located the global minima for $CysH^+$ and $[Cys\text{-}H]^-$ in their conformal landscapes.[9,11] Starting geometries of $CysH^+(H_2O)_{1,2}$ and $[Cys\text{-}H]^-(H_2O)_{1,2}$ were obtained by adding water to all possible hydration sites in the lowest energy conformations of $CysH^+$ and $[Cys\text{-}H]^-$, respectively, and then optimized at B3LYP/6-311++G(d,p). A similar approach was used to build the hydration shell of other amino acids.[45,46] Four lowest energy conformations were found for $CysH^+(H_2O)$, as shown in Fig. 1. Their structures are distinguished from each other by appending letter to structures alphabetically, *e.g.*, $CysH^+(H_2O)$_a is the most stable conformation for $CysH^+(H_2O)$. Hydration energy, indicated in parentheses below each structure, was calculated by $E_{hydration} = E(\text{bare ion}) + nE(H_2O) - E(\text{cluster})$, where E(bare ion), $E(H_2O)$ and E(cluster) are the B3LYP/6-311++G(d,p) energies of dehydrated ion, water and hydrated cluster, respectively; and n is the number of water ligands. As depicted in Fig. 1, both the carboxyl and ammonium groups of $CysH^+$ offer binding sites for water. The water oxygen either binds to the –OH site of the carboxyl group with a $H_2O\cdots HOOC$ distance of 1.59 Å, or to one of the three –NH sites of the ammonium group with a $H_2O\cdots HN$ distance of 1.67–1.74 Å. The hydration energies of three –NH sites differ by a maximum of 0.14 eV, and the hydration energy of the –OH site is only 0.02 eV less than that of the strongest –NH site.

Structures $CysH^+(H_2O)_2$_a–f in Fig. 1 represent addition of the second water molecule to each of the four $CysH^+(H_2O)$ conformers described above. The most stable dihydrated conformer, $CysH^+(H_2O)_2$_a, has two water molecules hydrogen bound to –NH and –OH, respectively. Note that the two H_2O molecules in $CysH^+(H_2O)_2$_a occupy the hydration sites of $CysH^+(H_2O)$_a and b simultaneously, but with the total hydration energy (1.33 eV) 0.05 eV less than the sum of $CysH^+(H_2O)$_a (0.70 eV) and $CysH^+(H_2O)$_b (0.68 eV). This phenomenon, also seen in other conformers of $CysH^+(H_2O)_2$, is due to decreasing effective charge on NH_3^+ and increasing repulsion between H_2O ligands.[26,47–49]

Before describing the structures of $[Cys\text{-}H]^-(H_2O)_{1,2}$, it is necessary to address the fact that Cys has two deprotonation sites, the carboxyl and thiol groups. pK_a of the carboxyl group (2.0) is 6.2 units smaller than that of the thiol group (8.2),[50] indicating that $[Cys\text{-}H]^-$ should be a carboxylate in solution. However, disputes arose regarding the structure of $[Cys\text{-}H]^-$ in the gas phase. Woo *et al.* claimed that ESI of Cys in methanol–water produced a thiolate in the gas phase according to photoelectron spectroscopy measurements.[51] Tian *et al.* also found that the preferred deprotonation site for gaseous Cys is the thiol side chain based on H/D exchange of $[Cys\text{-}H]^-$ with deuterated alcohols.[52] On the other hand, Oomens *et al.*[53] reported the gas-phase infrared multiple photon dissociation (IRMPD) spectrum of $[Cys\text{-}H]^-$ which was generated by ESI of a mixture of Cys and NaOH in methanol–water. The conformation-specific IRMPD spectrum identified a carboxylate structure only for gaseous $[Cys\text{-}H]^-$. It therefore seems that the structure of $[Cys\text{-}H]^-$ present in the gas phase depends on experimental conditions.[53] A similar finding was reported for the carboxylate *vs.* phenoxide structures of gaseous deprotonated Tyr.[10,53–55] In our CID experiments of $[Cys\text{-}H]^-$ and $[Cys\text{-}H]^-(H_2O)_{1,2}$ with Ar and $^3O_2$, dominant product ions include HS^- at m/z 33. HS^- is a characteristic fragment of the carboxylate structure, as reported in IRMPD.[53] This evidence leads us to conclude that our ESI source produced dominantly carboxylate structures for $[Cys\text{-}H]^-$ and $[Cys\text{-}H]^-(H_2O)_{1,2}$. For clarity, $HSCH_2CH(NH_2)CO_2^-$ was used to denote $[Cys\text{-}H]^-$ in the following discussion.

Four conformers were identified for each of $HSCH_2CH(NH_2)CO_2^-(H_2O)$ and $HSCH_2CH(NH_2)CO_2^-(H_2O)_2$. As shown in Fig. 1, their structures can be distinguished by hydrogen bonding motifs. The most stable monohydrated conformer, $HSCH_2CH(NH_2)CO_2^-(H_2O)$_a, undergoes bidentate complexation, forming two hydrogen bonds between H_2O and the carboxylate group in a six-membered cyclic arrangement,[45,46,56,57] with a hydration energy of 0.65 eV. Other three monohydrated conformers are mono-dentate complexes, each forming a hydrogen bond between H_2O and the carboxylate or amino group, with their hydration energies 0.09–0.21 eV less than that of $HSCH_2CH(NH_2)CO_2^-(H_2O)$_a. In conformers $HSCH_2CH(NH_2)CO_2^-(H_2O)$_c and d, the water molecule bridges $-COO^-$ and $-NH_2$, and–NH_2 and –SH, respectively. Shared proton binding motifs also occur between $-NH_2$ and $-COO^-$ in $HSCH_2CH(NH_2)CO_2^-(H_2O)$_a, b and d, and between the N atom and –SH in $HSCH_2CH(NH_2)CO_2^-(H_2O)$_a, b and c. No conformer was found with the water oxygen atom

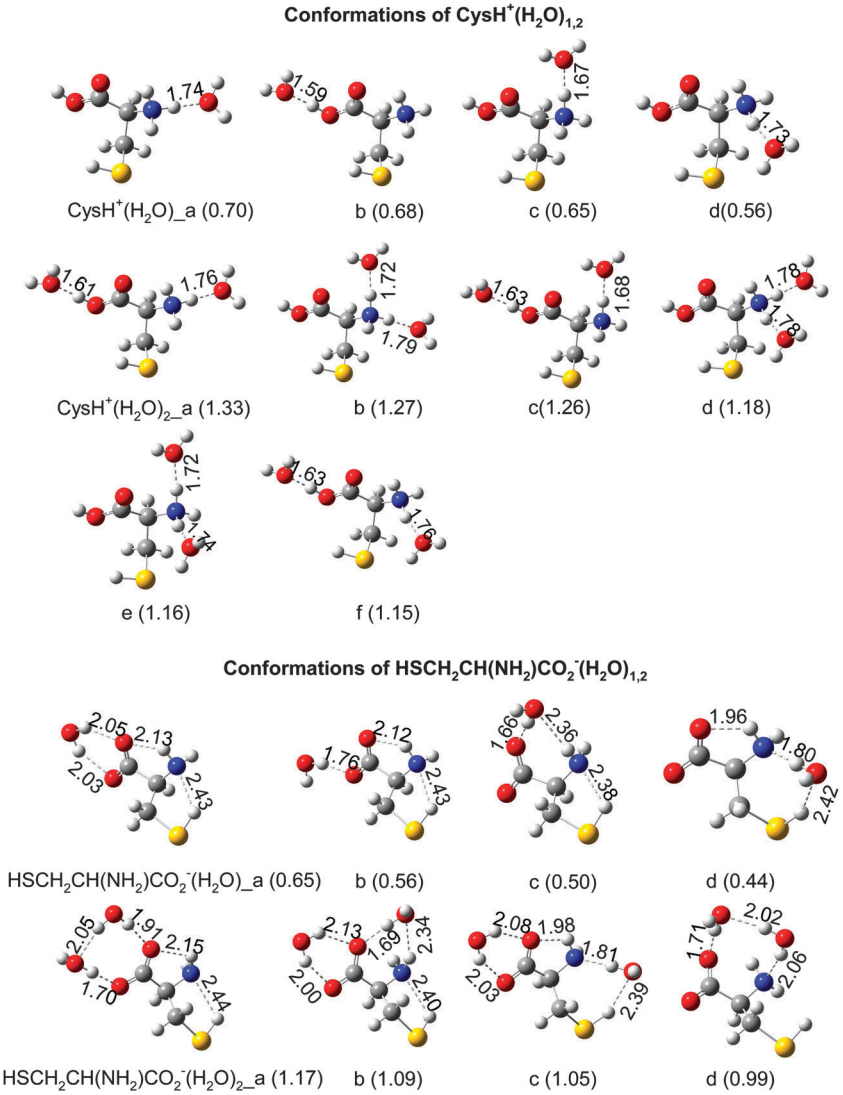

Fig. 1 Conformations of $CysH^+(H_2O)_{1,2}$ and $HSCH_2CH(NH_2)CO_2^-(H_2O)_{1,2}$ calculated at B3LYP/6-311++G(d,p). Dashed lines indicate hydrogen bonds. Bond distances are in Å. Hydration energies at 0 K (eV, including ZPE) are indicated in parentheses.

strongly bonded to an amino hydrogen atom such as in $CysH^+(H_2O)$_a.

$HSCH_2CH(NH_2)CO_2^-(H_2O)_2$_a represents the lowest energy conformer for dihydrated deprotonated Cys, in which two water molecules form two hydrogen bonds to carboxylate oxygen atoms, plus a weaker one between two waters. In $HSCH_2CH(NH_2)CO_2^-(H_2O)_2$_b and c, one water simultaneously binds to both oxygen atoms of $-COO^-$ in a manner similar to that in $HSCH_2CH(NH_2)CO_2^-(H_2O)$_a, and the other water bridges the C- and N-terminus, or the $-NH_2$ and –SH. $HSCH_2CH(NH_2)CO_2^-(H_2O)_2$_d has both water molecules inserted between the C- and N-terminus. Since this conformer is not able to include –SH in an intramolecular hydrogen bond, it has the lowest hydration energy.

Our calculations indicate that protonated and deprotonated Cys have distinctly different hydration structures. Protonated Cys has higher hydration energy than the deprotonated one, presumably due to the higher positive charge density centered on $-NH_3^+$ than the diffusive negative charge density on $-CO_2^-$.[57,58] Similar to $CysH^+$, $HSCH_2CH(NH_2)CO_2^-$ has higher binding energy with the first water, while the second water is less strongly bound by 18–38% due to charge delocalization over the water molecules.

3.2 Reaction cross sections

A. $CysH^+(H_2O)_{1,2}$ + $^1O_2$. For the reaction of $CysH^+(H_2O)$ (m/z 140) with $^1O_2$, product ions were observed at m/z 74, 93, 107, 122, 131 and 154 over the E_{col} range of 0.05–1.0 eV. Product ions of m/z 93, 107 and 122 correspond to elimination of CH_2SH, HS and H_2O from $CysH^+(H_2O)$, respectively, of which dissociation of $CysH^+(H_2O)$ to $CysH^+$ and H_2O is the most significant CID channel. Product ions of m/z 131, with an insignificant intensity, can be attributed to the formation of $(CysH^+)_2H_2O$. These products were also observed upon collisions of $CysH^+(H_2O)$ with $^3O_2$/He, and therefore could be excluded from $^1O_2$-specific reactions. Product ions of m/z 154, on the other hand, were not observed with $^3O_2$/He. m/z 154 corresponds to

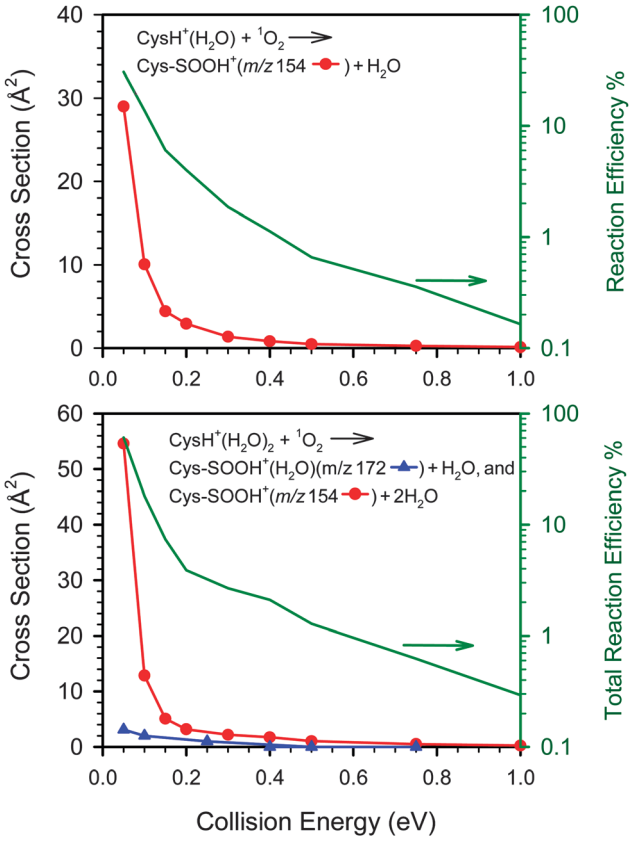

Fig. 2 Product cross sections for the reactions of $CysH^+(H_2O)_{1,2}$ with $^1O_2$, as a function of center-of-mass E_{col}. Reaction efficiencies are shown on the right axis.

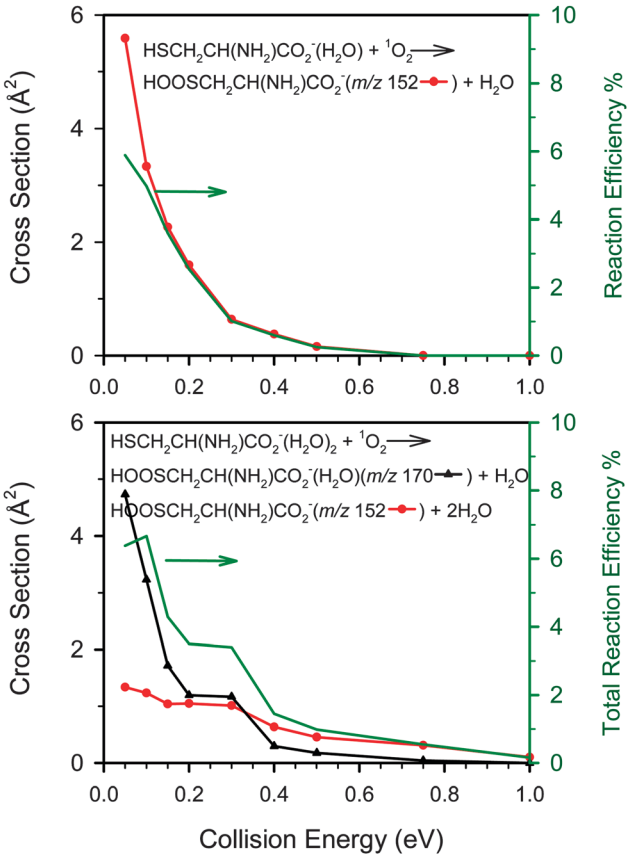

Fig. 3 Product cross sections for the reactions of $HSCH_2CH(NH_2)CO_2^-(H_2O)_{1,2}$ with $^1O_2$, as a function of center-of-mass E_{col}. Reaction efficiencies are shown on the right axis.

the formation of a hydroperoxide $Cys\text{-}SOOH^+$, and its cross section is shown in the top frame of Fig. 2 as a function of E_{col}. Also shown in Fig. 2 is the reaction efficiency (right-hand scale), calculated as $\sigma_{reaction}/\sigma_{collision}$. At low collision energies, $CysH^+$ formed from CID underwent secondary reaction with $^1O_2$, forming product ions of $H_2NCHCO_2H^+$ at m/z 74.[9]

For the reaction of $CysH^+(H_2O)_2$ (m/z 158) + $^1O_2$, product ions were observed at m/z 74, 93, 107, 122, 131, 140, 154 and 172. Products ions of m/z 74, 93, 107, 122, and 131 have the same origins as those observed in the reaction of $CysH^+(H_2O)$ + $^1O_2$, product ions of m/z 140 can be attributed to elimination of a H_2O molecule from $CysH^+(H_2O)_2$. Only m/z values of 154 and 172 belong to $^1O_2$-specific hydroperoxide products, of which m/z 172 corresponds to a monohydrated hydroperoxide $Cys\text{-}SOOH^+(H_2O)$ albeit its intensity is significantly lower than that of m/z 154 (*i.e.*, $Cys\text{-}SOOH^+$). Their cross sections and total reaction efficiency (sum of m/z 154 and 172) are shown in the bottom frame of Fig. 2 as a function of E_{col}.

Reactions of both $CysH^+(H_2O)$ and $CysH^+(H_2O)_2$ are significant only at low energies. Reaction efficiencies for $CysH^+(H_2O)$ and $CysH^+(H_2O)_2$ are 30% and 60%, respectively, at E_{col} = 0.05 eV, dropping to 6% and 7% at E_{col} = 0.2 eV, and becoming negligible at $E_{col} \geq 0.5$ eV. The rapid drop-off in the reaction efficiencies shown in Fig. 2 (and Fig. 3) reflects the inefficiency of the initial capture of the reactants before the energy can become dispersed among the internal modes of intermediates. Such collision energy dependence suggests that reactions are complex-mediated, with complex formation probabilities and/or lifetimes that are strongly suppressed by E_{col}. Another interesting observation is that the reaction of $CysH^+(H_2O)_2$ is more efficient than that of $CysH^+(H_2O)$, particularly at low E_{col}.

B. $HSCH_2CH(NH_2)CO_2^-(H_2O)_{1,2}$ + $^1O_2$. $^1O_2$-specific product ions were observed at m/z 152 for $HSCH_2CH(NH_2)CO_2^-(H_2O)$ (m/z 138) + $^1O_2$, and at m/z 152 and 170 for $HSCH_2CH(NH_2)CO_2^-(H_2O)_2$ (m/z 156) + $^1O_2$. Their reaction cross sections and efficiencies as well as E_{col} dependence are shown in Fig. 3. Similar to $CysH^+(H_2O)_{1,2}$ + $^1O_2$, reactions of $HSCH_2CH(NH_2)CO_2^-(H_2O)_{1,2}$ + $^1O_2$ are strongly inhibited by collision energies (note that a similar E_{col} dependence of reaction efficiency was observed for the reactions of $^1O_2$ with dehydrated $CysH^+$ and $HSCH_2CH(NH_2)CO_2^-$ (ref. 9 and 11)). However, reaction efficiencies of $HSCH_2CH(NH_2)CO_2^-(H_2O)$ and $HSCH_2CH(NH_2)CO_2^-(H_2O)_2$ are only one-fifth and one-tenth, respectively, compared to their protonated counterparts.

In addition to $^1O_2$-specific product ions, we have observed CID product ions of $HSCH_2CH(NH_2)CO_2^-(H_2O)$ and $HSCH_2CH(NH_2)CO_2^-(H_2O)_2$ at m/z 33 (HS^-), 76 (elimination of CO_2 + H_2O from $HSCH_2CH(NH_2)CO_2^-(H_2O)$), 120 and 138 (elimination of a H_2O molecule from $HSCH_2CH(NH_2)CO_2^-(H_2O)$ and $HSCH_2CH(NH_2)CO_2^-(H_2O)_2$, respectively), and 102 (elimination of H_2O from the primary fragment $HSCH_2CH(NH_2)CO_2^-$), as well as formation of the dimer $(HSCH_2CH(NH_2)CO_2^-)_2H_2O$

at m/z 129 (insignificant intensity). In contrast to product ions of m/z 152 and 170, these product ions were observed in the control experiment with $^3O_2$/He, and their intensities increase at high collision energies. Since these products are not relevant to $^1O_2$ chemistry, they are not discussed further.

Note that the electron detachment energy for $HSCH_2CH(NH_2)CO_2^-(H_2O)$/$HSCH_2CH(NH_2)CO_2^-(H_2O)_2$ is 2.92/3.26 eV, calculated at B3LYP/6-311++G(d,p), which is beyond the E_{col} range of 0.05–1.0 eV used in our experiment. Consequently, collision-induced detachment of an excess electron from $HSCH_2CH(NH_2)CO_2^-(H_2O)$/$HSCH_2CH(NH_2)CO_2^-(H_2O)_2$ could be disregarded. In addition, assuming all of the excitation energy (0.98 eV)[36] and electron affinity (0.45 eV)[59] of $^1O_2$ can be used for reactions, electron transfer between $HSCH_2CH(NH_2)CO_2^-(H_2O)$/$HSCH_2CH(NH_2)CO_2^-(H_2O)_2$ and $^1O_2$ is endothermic by 1.49/1.83 eV, and thus cannot occur in our E_{col} range, either.

3.3 Reaction mechanisms

A. $CysH^+(H_2O)_{1,2}$ + $^1O_2$. Among the conformers of $CysH^+(H_2O)$ presented in Fig. 1, $CysH^+(H_2O)$_a and b are predicted to have a population of 62% and 29%, respectively, while $CysH^+(H_2O)$_c and d have a total population of 9% under our experimental conditions. Among the $CysH^+(H_2O)_2$ conformers, $CysH^+(H_2O)_2$_a has the largest population (>85%), while the rest of the conformers account for less than 15%. Based on the significance of their populations, we chose conformers $CysH^+(H_2O)$_a and b as the reactant structures for monohydrated $CysH^+$, and $CysH^+(H_2O)_2$_a for dihydrated $CysH^+$, respectively, for construction of their reaction coordinates. To differentiate the water binding sites in $CysH^+(H_2O)$_a and b, we include the termini to which water binds in the formulas, *i.e.*, $CysH^+(H_2O)$_a is referred to as $CysH^+(N\text{-}H_2O)$, and $CysH^+(H_2O)$_b as $CysH^+(C\text{-}H_2O)$, for clarity, in the discussion of reaction mechanisms.

In a previous study, we have proposed a mechanism for the reaction of bare $CysH^+$ with $^1O_2$, which involves formation of a hydroperoxide intermediate Cys-$SOOH^+$.[9] Considering the similarities between the chemistry of $CysH^+$ and its hydrated analogues, we may reasonably presume that m/z 154 and 172 correspond to formation of similar hydroperoxides from $CysH^+(H_2O)$/$CysH^+(H_2O)_2$ + $^1O_2$. Their structures are shown in Fig. 4, and reaction enthalpies calculated at B3LYP/6-31+G(d) are as follows:

$$CysH^+(N\text{-}H_2O) + {}^1O_2 \rightarrow \text{Cys-}SOOH^+ + H_2O \quad \Delta H = -1.27 \text{ eV} \quad (1a)$$

$$CysH^+(C\text{-}H_2O) + {}^1O_2 \rightarrow \text{Cys-}SOOH^+ + H_2O \quad \Delta H = -1.30 \text{ eV} \quad (1b)$$

$$CysH^+(H_2O)_2 + {}^1O_2 \rightarrow \text{Cys-}SOOH^+(C\text{-}H_2O) + H_2O \quad \Delta H = -1.30 \text{ eV} \quad (2a)$$

$$\rightarrow \text{Cys-}SOOH^+(N\text{-}H_2O) + H_2O \quad \Delta H = -1.32 \text{ eV} \quad (2b)$$

$$\rightarrow \text{Cys-}SOOH^+(S\text{-}H_2O) + H_2O \quad \Delta H = -1.11 \text{ eV} \quad (2c)$$

$$\rightarrow \text{Cys-}SOOH^+ + 2H_2O \quad \Delta H = -0.63 \text{ eV} \quad (2d)$$

Fig. 4 presents potential energy surfaces (PESs) associated with possible low energy reaction pathways for $CysH^+(N\text{-}H_2O)$ + $^1O_2$ and $CysH^+(C\text{-}H_2O)$ + $^1O_2$, respectively, with the reactants shown at zero energy. Energies of complexes, TSs and products are derived from B3LYP/6-31+G(d) calculations, except for that of TS2(N-H_2O) which was calculated at B3LYP/aug-cc-pVQZ and compared to the energy of the reactants at the same basis set. Note that due to the mixing of open- and closed-shell characteristics of $^1O_2$, the standard DFT method overestimates the electronic excitation energy of $^1O_2$.[60] In our calculations, the DFT energy of $^1O_2$ was obtained by adding the experimental excitation energy of 0.98 eV (ref. 36) to the DFT energy of $^3O_2$.

We first focus on the reaction coordinate for $CysH^+(N\text{-}H_2O)$ + $^1O_2$, as displayed in Fig. 4a. One weakly bound complex PC(N-H_2O), and several covalently bound complexes, *i.e.*, $CysOOH^+(N\text{-}H_2O)$, $CysOOH^+(N\text{-}H_2O)'$, $CysOOH^+(S\text{-}H_2O)$, Cys-$SOOH^+(N\text{-}H_2O)$ and Cys-$SOOH^+(S\text{-}H_2O)$, were identified. The transition states (TSs) connecting the complexes to each other and to the products are indicated in the figure. PC(N-H_2O) can be characterized as a reactant-like complex, formed by electrostatic interaction and hydrogen bonding between $CysH^+(N\text{-}H_2O)$ and O_2. It has the O_2 moiety sandwiched between the thiol and ammonium groups of $CysH^+$, with distances of 2.39 and 1.71 Å for HS···O–O and O–O···HN, respectively. The binding energy of PC(N-H_2O) is 0.05 eV with respect to the reactants. Because no rearrangement is needed to form this reactant-like complex from the reactants, it is less likely to have a significant barrier inhibiting formation of PC(N-H_2O). This was verified by trajectory simulations to be discussed below. Because of a lack of directional covalent bonds between $CysH^+(N\text{-}H_2O)$ and O_2 moieties, PC(N-H_2O) does not have a well-defined geometry at the energies available in our experiment, and is rather floppy with a large amplitude of intermolecular motion as seen in trajectories (*vide infra*). The point is that PC(N-H_2O) allows repeated encounters between reactants, increasing reaction probability for collisions not initially in the correct geometry. To this extent, complex PC(N-H_2O) acts as a "precursor complex".

The precursor complex may undergo intramolecular proton transfer from $-NH_3$ to the peroxide group through TS1(N-H_2O), leading to formation of a persulfoxide $CysOOH^+(N\text{-}H_2O)$. $CysOOH^+(N\text{-}H_2O)$ is a covalently bound intermediate, with a binding energy of 0.36 eV relative to the reactants. $CysOOH^+(N\text{-}H_2O)$ may then converge to a more stable hydroperoxide intermediate Cys-$SOOH^+(N\text{-}H_2O)$ *via* TS2(N-H_2O). During the interconversion from $CysOOH^+(N\text{-}H_2O)$ to Cys-$SOOH^+(N\text{-}H_2O)$, the proton initially abstracted by the –SOO group returns to the $-NH_2$ group; simultaneously a H atom is transferred from the –SH group to the oxygen end of –SOO. The overall reaction pathway is outlined by black lines in Fig. 4a, *i.e.* $CysH^+(N\text{-}H_2O)$ + $^1O_2$ → PC(N-H_2O) → TS1(N-H_2O) → $CysOOH^+(N\text{-}H_2O)$ → TS2(N-H_2O) → Cys-$SOOH^+(N\text{-}H_2O)$ → Cys-$SOOH^+$ (m/z 154) + H_2O, and referred to as pathway a. The reaction enthalpy for pathway a is −1.27 eV, and all associated TSs are below the reactants, consistent with our experimental observation of an exothermic reaction. In principle, product ions of m/z 154 could be $CysOOH^+$ and/or $CysOOH^{+\prime}$ (indicated by gray lines on the top right of Fig. 4a), which may be produced by elimination of water from $CysOOH^+(N\text{-}H_2O)$. However, the reaction enthalpy for $CysOOH^+$ (0.14 eV) as well as the barrier at TS3 (0.47 eV)

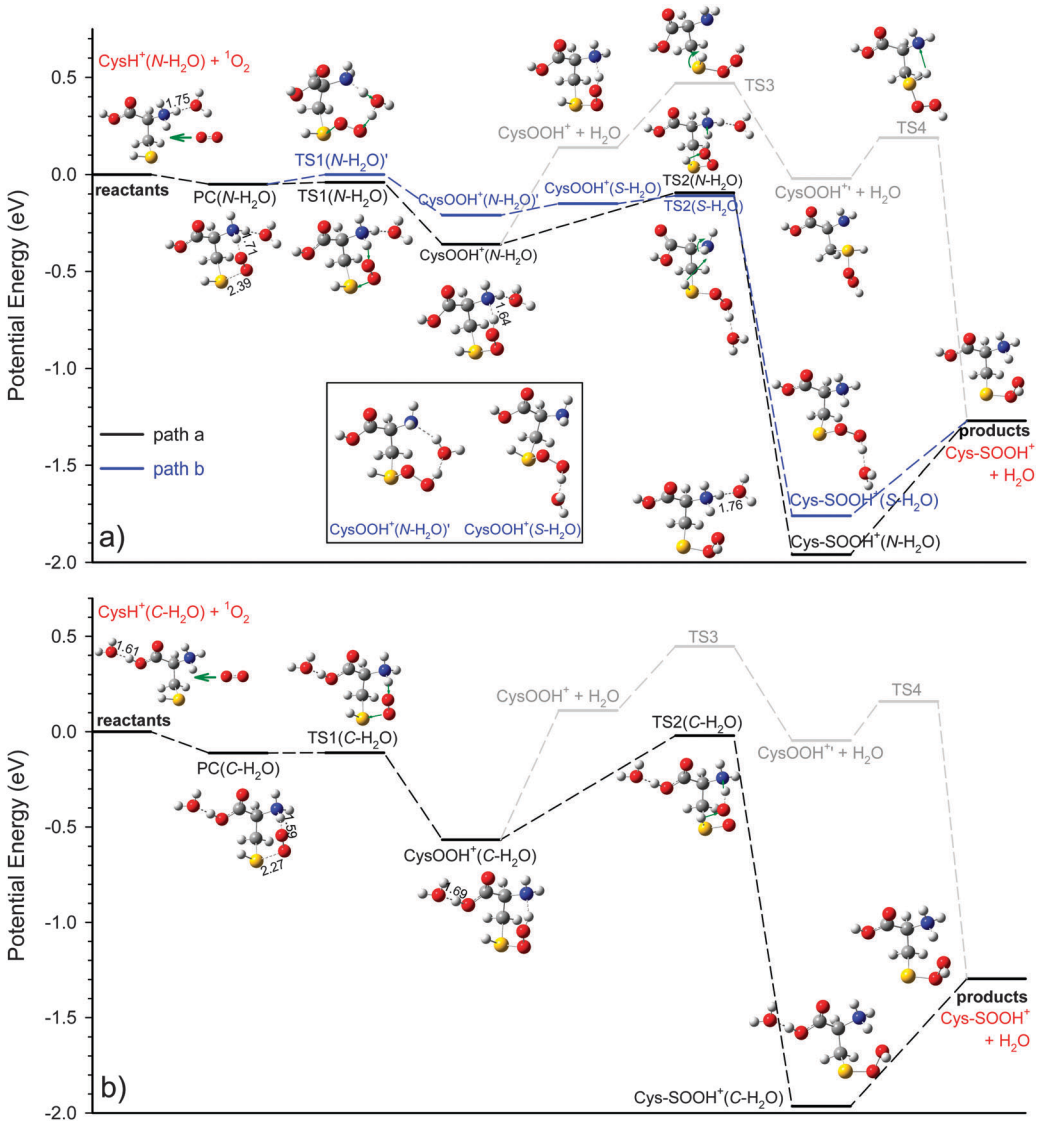

Fig. 4 Schematic reaction coordinate for $^1O_2$ with (a) $CysH^+(N\text{-}H_2O)$ and (b) $CysH^+(C\text{-}H_2O)$. Structures of $CysOOH^+$, $CysOOH^{+\prime}$, TS3 and TS4 in (b) are identical to those in (a). Energies of complexes, TSs, and products, relative to reactants, are derived from B3LYP/6-31+G(d) and B3LYP/aug-cc-pVQZ results. Bond distances are in Å. For TSs, vibrational modes corresponding to imaginary frequencies are indicated by displacement vectors.

leading to $CysOOH^{+\prime}$ render formation of these ion structures improbable at low E_{col}.

Note that in pathway a, the water ligand acts as a spectator until its elimination at the last step. There exists an alternative pathway b in which the water ligand catalyzes the reaction. Pathway b was revealed by trajectory simulations where the motion of molecules is followed, allowing the molecules to show what the preferred reaction pathways are. This pathway is outlined by blue lines in Fig. 4a, corresponding to $CysH^+(N\text{-}H_2O) + {}^1O_2 \rightarrow PC(N\text{-}H_2O) \rightarrow TS1(N\text{-}H_2O)' \rightarrow CysOOH^+(N\text{-}H_2O)' \rightarrow CysOOH^+(S\text{-}H_2O) \rightarrow TS2(S\text{-}H_2O) \rightarrow Cys\text{-}SOOH^+(S\text{-}H_2O) \rightarrow Cys\text{-}SOOH^+ + H_2O$. One unique feature of pathway b is that water is intimately involved in the reaction. At $TS1(N\text{-}H_2O)'$, the water accepts a proton from $-NH_3$ and in the meantime donates another to –SOO, leading to formation of $CysOOH^+(N\text{-}H_2O)'$. $CysOOH^+(S\text{-}H_2O)$, where the "*S*" denotes the side chain to which water binds, is an analogue of $CysOOH^+(N\text{-}H_2O)'$ except that the water ligand swings from $-NH_2$ to –SOOH. The activation barrier (not included in Fig. 4a) for the interconversion between these two peroxides is minuscule (only 0.07 eV above $CysOOH^+(S\text{-}H_2O)$). The energy of $CysOOH^+(S\text{-}H_2O)$ is slightly higher than that of $CysOOH^+(N\text{-}H_2O)'$, presumably because of the absence of a $-NH_2\cdots$water hydrogen bond in $CysOOH^+$-$(S\text{-}H_2O)$. $CysOOH^+(S\text{-}H_2O)$ may transfer a H atom from S to $-NH_2$ *via* $TS2(S\text{-}H_2O)$, yielding $Cys\text{-}SOOH^+(S\text{-}H_2O)$ followed by dissociation to $Cys\text{-}SOOH^+ + H_2O$. While pathways a and b yield identical products, intramolecular proton transfer in pathway a *vs.* water-assisted proton transfer in pathway b leads to different PESs.

Fig. 4b shows the PES for $CysH^+(C\text{-}H_2O) + {}^1O_2$. This reaction follows a similar route to pathway a for $CysH^+(N\text{-}H_2O) + {}^1O_2$, *i.e.*, $CysH^+(C\text{-}H_2O) + {}^1O_2 \rightarrow PC(C\text{-}H_2O) \rightarrow TS1(C\text{-}H_2O) \rightarrow CysOOH^+(C\text{-}H_2O) \rightarrow TS2(C\text{-}H_2O) \rightarrow Cys\text{-}SOOH^+(C\text{-}H_2O) \rightarrow Cys\text{-}SOOH^+$ (m/z 154) + H_2O, with an overall reaction enthalpy

of −1.30 eV. We did not run trajectory simulations for $CysH^+$-(*C*-H_2O). But it seems less likely to have water assist the reaction in PC(*C*-H_2O) since the water ligand binds to a place opposite to the reaction center. Similar to $CysH^+$(*N*-H_2O) + $^1O_2$, product ions of $CysOOH^+$ and $CysOOH^{+\prime}$ could be ruled out for $CysH^+$-(*C*-H_2O) + $^1O_2$ due to their high endothermicities.

Computation results for $CysH^+(H_2O)_2$ + $^1O_2$ at B3LYP/6-31+G(d) level are summarized in Fig. 5. One of the minimum energy paths leading to Cys-$SOOH^+$(*C*-H_2O) and/or Cys-$SOOH^+$-(*N*-H_2O) is $CysH^+(H_2O)_2$ + $^1O_2$ → $PC(H_2O)_2$ → $TS1(H_2O)_2$ → $CysOOH^+(H_2O)_2$ → $TS2(H_2O)_2$ → Cys-$SOOH^+(H_2O)_2$ → Cys-$SOOH^+$(*N*-H_2O)/Cys-$SOOH^+$(*C*-H_2O) (*m*/*z* 172) + H_2O, of which $TS1(H_2O)_2$ and $TS2(H_2O)_2$ are located 0.05 and 0.1 eV below the reactants, respectively. Since one water ligand in $CysH^+(H_2O)_2$ is bound to a –NH site, there exists another pathway relying on water-assisted proton transfer, as pathway b for $CysH^+$(*N*-H_2O). This is outlined by blue lines in Fig. 5 as $CysH^+(H_2O)_2$ + $^1O_2$ → $PC(H_2O)_2$ → $TS1(H_2O)_2'$ → $CysOOH^+(H_2O)_2'$ → $CysOOH^+$-$(H_2O)_2''$ →$TS2(H_2O)_2'$ → Cys-$SOOH^+(H_2O)_2'$ → Cys-$SOOH^+$-(*S*-H_2O)/Cys-$SOOH^+$(*C*-H_2O) (*m*/*z* 172) + H_2O. Note that the water-assisted pathways for $CysH^+$(*N*-H_2O) and $CysH^+(H_2O)_2$ are extremely alike in PES and energetics.

As mentioned above, $CysH^+(H_2O)_2$ + $^1O_2$ has higher reaction efficiency than $CysH^+(H_2O)$ + $^1O_2$ (see Fig. 2). This observation might be attributed to two facts. First, density of vibrational states in the dihydrated system is higher than that in the monohydrated system, and so the intramolecular vibrational relaxation is faster for prompt dissociation of Cys-$SOOH^+(H_2O)_2$. Second, since the second water is less strongly bound than the first one, the dihydrated cluster has a lower energy dissociation channel to eject water than the monohydrated one.

Fig. 5 includes two alternative structures for *m*/*z* 172, *i.e.*, $CysOOH^+$(*N*-H_2O) and $CysOOH^+$(*C*-H_2O). But reaction enthalpies of $CysOOH^+$(*N*-H_2O) and $CysOOH^+$(*C*-H_2O) suggest that they are not significant at low E_{col}. Finally, a large fraction of monohydrated Cys-$SOOH^+$(*N*-H_2O), Cys-$SOOH^+$(*C*-H_2O) and Cys-$SOOH^+$-(*S*-H_2O) may undergo secondary reactions, eliminating the remaining water ligand. Consequently, Cys-$SOOH^+$ accounts for >85% of total product ions at $E_{col} \leq 0.1$ eV.

B. $HSCH_2CH(NH_2)CO_2^-(H_2O)_{1,2}$ + $^1O_2$. Based on their relative energies, $HSCH_2CH(NH_2)CO_2^-(H_2O)$_a accounts for 97% of monohydrated while $HSCH_2CH(NH_2)CO_2^-(H_2O)_2$_a accounts for 95% of dihydrated deprotonated Cys under our experimental conditions. Therefore, these two conformers were used as the reactant ion structures for construction of the reaction coordinates for $HSCH_2CH(NH_2)CO_2^-(H_2O)$ and $HSCH_2CH(NH_2)CO_2^-$-$(H_2O)_2$, respectively. Their reaction enthalpies calculated at B3LYP/6-31+G(d) are as follows,

$$HSCH_2CH(NH_2)CO_2^-(H_2O) + {}^1O_2 \rightarrow HOOSCH_2CH(NH_2)CO_2^- + H_2O \quad \Delta H = -1.24 \text{ eV} \tag{3}$$

$$HSCH_2CH(NH_2)CO_2^-(H_2O)_2 + {}^1O_2 \rightarrow HOOSCH_2CH(NH_2)CO_2^-(H_2O) + H_2O \quad \Delta H = -1.34 \text{ eV} \tag{4a}$$

$$\rightarrow HOOSCH_2CH(NH_2)CO_2^- + 2H_2O \quad \Delta H = -0.69 \text{ eV} \tag{4b}$$

PESs associated with possible low energy reaction pathways for $^1O_2$ with $HSCH_2CH(NH_2)CO_2^-(H_2O)$ and $HSCH_2CH(NH_2)CO_2^-$-$(H_2O)_2$ are presented in Fig. 6a and b, respectively. Since these two systems present very similar reaction behaviors, we describe their PESs together. Similar to $CysH^+(H_2O)_{1,2}$, $HSCH_2CH(NH_2)$-$CO_2^-(H_2O)_{1,2}$ may form precursor complexes with $^1O_2$, *i.e.*, $PC^-(H_2O)_{1,2}$. Their binding energies are 0.67 and 0.63 eV, respectively, with regard to the corresponding reactants. $PC^-(H_2O)_{1,2}$ goes through two consecutive TSs ($TS1a^-(H_2O)_{1,2}$ and $TS1b^-(H_2O)_{1,2}$).

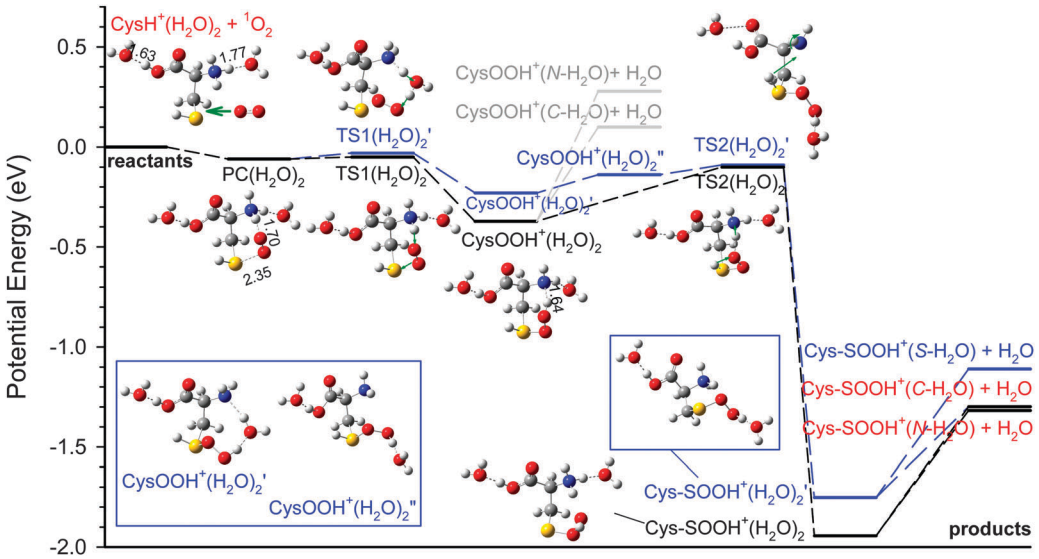

Fig. 5 Schematic reaction coordinate for $CysH^+(H_2O)_2$ with $^1O_2$ (elimination of the second water is not shown). Energies of complexes, TSs, and products, relative to reactants, are derived from a combination of B3LYP/6-31+G(d) results. Bond distances are in Å. For TSs, vibrational modes corresponding to imaginary frequencies are indicated by displacement vectors.

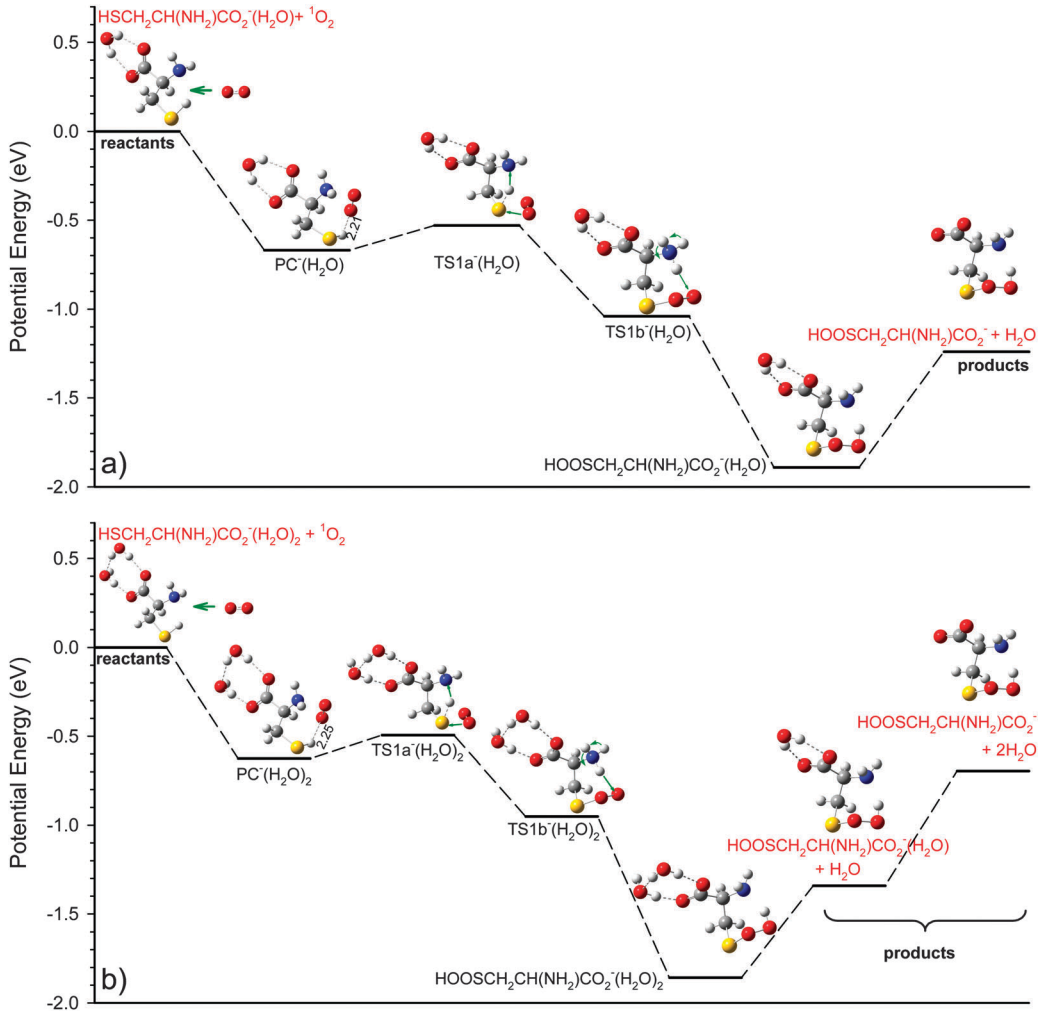

Fig. 6 Schematic reaction coordinate for $^1O_2$ with (a) $HSCH_2CH(NH_2)CO_2^-(H_2O)$ and (b) $HSCH_2CH(NH_2)CO_2^-(H_2O)_2$. Energies of complexes, TSs, and products, relative to reactants, are derived from B3LYP/6-31+G(d) results. Bond distances are in Å. For TSs, vibrational modes corresponding to imaginary frequencies are indicated by displacement vectors.

At $TS1a^-(H_2O)_{1,2}$, which corresponds to a barrier slightly above $PC^-(H_2O)_{1,2}$, the H atom of the thiol group is transferred to the amino group, and the O_2 moiety starts binding to the S atom. The path from $TS1a^-(H_2O)_{1,2}$ leads to $TS1b^-(H_2O)_{1,2}$, in which the same H atom now moves from $-NH_3$ to the other end of the O_2 moiety, leading to formation of a hydroperoxide complex $HOOSCH_2CH(NH_2)CO_2^-(H_2O)_{1,2}$. $HOOSCH_2CH(NH_2)CO_2^-(H_2O)$ and $HOOSCH_2CH(NH_2)CO_2^-(H_2O)_2$ may liberate a water molecule to yield product ions of $HOOSCH_2CH(NH_2)CO_2^-$ (m/z 152) and $HOOSCH_2CH(NH_2)CO_2^-(H_2O)$ (m/z 170), respectively. For $HSCH_2CH(NH_2)CO_2^-(H_2O)_2 + {}^1O_2$, both $HOOSCH_2CH(NH_2)CO_2^-$ and $HOOSCH_2CH(NH_2)CO_2^-(H_2O)$ were observed experimentally; however, in contrast to what was seen in the reaction of $CysH^+(H_2O)_2$, oxidation of $HSCH_2CH(NH_2)CO_2^-(H_2O)_2$ produced more hydrated product ions $HOOSCH_2CH(NH_2)CO_2^-(H_2O)$ than dehydrated ones.

3.4 Direct dynamics trajectory simulations of $CysH^+(N\text{-}H_2O) + {}^1O_2$

A further understanding of the collision dynamics for $CysH^+(N\text{-}H_2O) + {}^1O_2$ was obtained by examining their trajectories at E_{col} = 0.1 and 0.2 eV. One hundred trajectories were completed at each E_{col}. All trajectories were calculated at b = 0.1 Å using the B3LYP/4-31G(d) level. While a few trajectories completed reactions within trajectory simulation times (3–5 ps), the majority of the trajectories form precursor complexes and become trapped in that potential energy well. The remaining trajectories belong to non-reactive collisions, *i.e.*, fly-by without forming long-lasting complexes.

Fig. 7a demonstrates a trajectory representative of nonreactive collisions. The plots show the changes in potential energy (PE) and CM distances along trajectory simulation time. The CM distances are the distances between the centers of mass of $^1O_2$ and $CysH^+$, and of H_2O and $CysH^+$, respectively. This trajectory represents a direct scattering, with only one turning point in the relative motion of $^1O_2$ *vs.* $CysH^+$, *i.e.*, there is no sign of complex-mediation; in addition, the water ligand remains bound to $CysH^+$ during the collision as indicated by the change in $r(H_2O\text{–}CysH^+)$. The time scale of the collision is somewhat arbitrary, but two numbers are relevant. The time between the start of the trajectory and the onset of strong interaction, which depends on the reactant orientation, is around 350 fs. The time taken for reactants to approach within 5 Å of CM

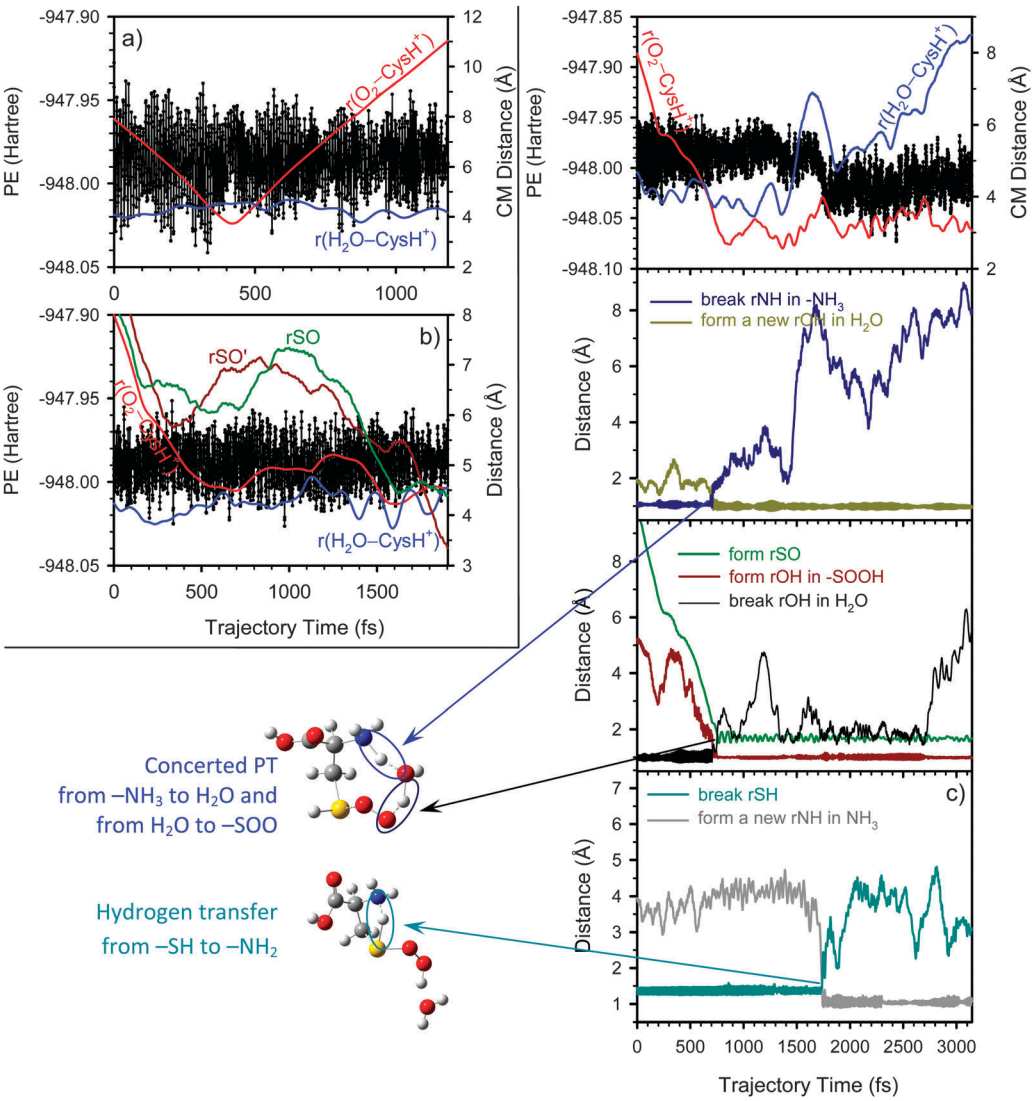

Fig. 7 Representative plots of a (a) nonreactive, (b) complex-forming, and (c) complete reactive trajectory at E_{col} = 0.1 eV. Trajectory (c) illustrates water-assisted proton transfer.

distance is around 250 fs. During the trajectory, PE fluctuates due to the vibrational motions of the reactants.

Fig. 7b illustrates a complex-forming trajectory, with the similar reactants approach time as that for the nonreactive trajectory. In addition to the changes in PE and the CM distances r(O_2–CysH$^+$) and r(H_2O–CysH$^+$), Fig. 7b shows the approaching of the O_2 moiety toward the S atom as indicated by the distances between S and two O atoms of O_2, *i.e.*, rSO and rSO′. This trajectory initially forms a loosely bound complex as shown by the decrease of r(O_2–CysH$^+$) to less than 5 Å starting at 450 fs. The reactants have repeated encounters after their initial collision and remain close to each other. In agreement with the PES in Fig. 4a, no obvious potential barrier is observed during formation of the precursor complex. Toward the end of the trajectory, both rSO and rSO′ decrease rapidly, implying that the trajectory may ultimately lead to formation of a persulfoxide complex.

Finally, a trajectory producing Cys-SOOH$^+$ and a separated water molecule is depicted in Fig. 7c. The bonds plotted in Fig. 7c correspond to the N–H bonds being broken and formed in –NH_3, the O–H bonds being broken and formed in H_2O, the breaking thiol group, and the new O–H and S–O bonds being formed in the product Cys-SOOH$^+$, respectively. High frequency oscillations of various bonds reflect the vibrations of the reactants or products. Two middle frames of Fig. 7c show a concerted transfer of two protons at ~700 fs; one proton is transferred from –NH_3 to water, and simultaneously another from water to –SOO. At the same time, a persulfoxide bond is formed between the O_2 moiety and S, leading to CysOOH$^+$(*N*-H_2O). Around 1000 fs later, the H in the thiol group is transferred to the amino group and the water swings from –NH_3 to –SOOH, forming Cys-SOOH$^+$(*S*-H_2O). This trajectory verifies reaction pathway b we have proposed in Fig. 4a. Elimination of water occurs after completion of proton and hydrogen transfer. By the end of the trajectory, water is separated from Cys-SOOH$^+$ by 8.5 Å.

The simulations show that all persulfoxide and hydroperoxide complexes formed in trajectories did not decay back to

the reactants before the termination of the trajectories (typically 3–5 ps). This suggests that the lifetimes of these complexes are at least no less than the trajectory time. For comparison, the classical rotational period of a complex estimated using the average angular momentum is 2.5 ps at E_{col} = 0.1 eV. The fly-by time, taken as the time required for 5 Å motion at the relative speed of reactants, is 0.58 ps at E_{col} = 0.1 eV. The fly-by time gives a measure of how long a direct collision would last at the same E_{col}. Clearly, the complex lifetime is significantly longer than the fly-by time, and comparable to the complex rotational period. Note that one problem for the present system is that the combined lifetime of the precursor and peroxide complexes is too long to allow most trajectories to complete. But trajectories provide information concerning the early time dynamics; particularly, confirming complex mediation in the reaction.

3.5 Role of water molecules and its implication in mimicking solution-phase oxidation

Hydroperoxide complexes Cys-SOOH$^+$ and $HOOSCH_2CH(NH_2)CO_2^-$ have been formed during the reactions of $^1O_2$ with bare CysH$^+$ and $HSCH_2CH(NH_2)CO_2^-$,[9,11] respectively, as verified by trajectory simulations.[9,11] However, in those cases, nascent Cys-SOOH$^+$ ultimately decomposes to $H_2NCHCO_2H^+ + CH_3SH + {}^3O_2$ (with a dissociation energy of 0.67 eV), and $HOOSCH_2CH(NH_2)CO_2^-$ decomposes to $NH_2CH_2CO_2^- + CH_2S + {}^3O_2$ (with a dissociation energy of 2.12 eV). These dissociation reactions need to be driven by the $^1O_2$ excitation energy, the so-called dissociative excitation energy transfer.[61] Dissociative excitation energy transfer breaks the spin conservation rule, and therefore requires strong spin-orbital coupling within these complexes which could catalyze access to triplet channels.[9,11,61] However, the dissociative excitation energy transfer mechanism completely shuts off in hydrated ions. Instead, we have observed stable Cys-SOOH$^+$ and $HOOSCH_2CH(NH_2)CO_2^-$ products produced by elimination of water ligands from Cys-SOOH$^+(H_2O)_{1,2}$ and $HOOSCH_2CH(NH_2)CO_2^-(H_2O)_{1,2}$, respectively.

The key to unraveling this puzzle lies in the fact that ion clusters with weakly bound water provide a mechanism by which the energized hydroperoxide product complex can dispose of sufficient internal excitation so that the hydroperoxide moiety does not undergo further dissociation. The dissociation energies of Cys-SOOH$^+$(*N*-H_2O), Cys-SOOH$^+$(*C*-H_2O) and Cys-SOOH$^+$(*S*-H_2O) to Cys-SOOH$^+$ + H_2O are 0.69, 0.67 and 0.49 eV, respectively; while those of Cys-SOOH$^+(H_2O)_2$ to Cys-SOOH$^+$(*N*-H_2O) + H_2O, Cys-SOOH$^+$(*C*-H_2O) + H_2O and Cys-SOOH$^+$(*S*-H_2O) + H_2O are 0.62, 0.64 and 0.83 eV, respectively. Similar dissociation energies were found for $HOOSCH_2CH(NH_2)CO_2^-(H_2O)_{1,2}$. Therefore, Cys-SOOH$^+(H_2O)_{1,2}$ and $HOOSCH_2CH(NH_2)CO_2^-(H_2O)_{1,2}$ are expected to dissociate by loss of water molecule(s), and retain the structures of peroxide moieties. These dissociation reactions circumvent dynamical bottlenecks imposed by a spin-forbidden process (*i.e.*, formation of $^3O_2$), and should be more efficient. As a result, *just one water molecule could introduce a significant step in the transition of Cys oxidation from the gas phase to the solution*, and hydrated Cys ions generally have higher reaction efficiencies with $^1O_2$ than dehydrated Cys ions.

A complication in thinking about the reactions of hydrated clusters with $^1O_2$ is that the water ligands may physically quench $^1O_2$ during collisions. In the present experiment, we were not able to directly probe the physical quenching of $^1O_2$. The quasi-classical trajectory method we used cannot simulate the physical quenching of $^1O_2$, either, because trajectories were confined to the lowest energy singlet potential energy surface. However, trajectory simulations of CysH$^+(H_2O)$ + $^1O_2$ illustrate that at E_{col} = 0.1 eV, only less than 18% of collisions have $^1O_2$ attack the water ligand directly, and only a fraction of such collisions may actually quench $^1O_2$. Therefore, it is less likely that the physical quenching by water would significantly affect the branching of $^1O_2$ chemical reactions. An experiment using D_2O hydrated clusters could decrease the rate of physical quenching (the rate constant for $^1O_2$ quenching is 1.8×10^4 s^{-1} in D_2O solution *vs.* 2.4×10^5 s^{-1} in H_2O (ref. 62)), and may provide more insight into the relative physical *vs.* chemical quenching contributions in the collisions of hydrated Cys with $^1O_2$.

The above scheme may lead to an impression that the water in hydrated Cys clusters acts mostly as a spectator in reactions such as rare gas tagging (in rare gas-tagged clusters, rare gas atoms represent very weak perturbations to hosts, and spectra of rare gas-tagged clusters represent structures and dynamics of unperturbed systems).[63–65] However, this is not the case for oxidation of hydrated Cys. Trajectories show water-catalyzed proton transfer for CysH$^+$(*N*-H_2O) + $^1O_2$, demonstrating that the reaction coordinate of CysH$^+$ + $^1O_2$ can be altered by the absorbed water. This finding reinforces the understanding that gas-phase hydrated amino acids involve both solute and solvent dynamics and their coupling, rather than simply amino acid dynamics under the influence of some representation of the solvent.[66]

IV. Conclusions

Guided-ion-beam tandem mass spectrometry was employed to determine reaction products, cross sections and collision energy dependence for the reactions of $O_2(a^1\Delta_g)$ with mono- and dihydrated protonated/deprotonated Cys. DFT calculations were carried out to identify reaction coordinates, investigate thermodynamics and energy barriers. Quasi-classical, direct dynamics trajectory simulations were used to study the atomic-level mechanism of CysH$^+$(*N*-H_2O) + $^1O_2$. The combined experimental and theoretical investigation reveals the effects of hydration on Cys oxidation by $^1O_2$. It is found that hydrated systems are able to relax ''energized, unstable'' nascent hydroperoxide products by ''evaporating'' water ligand(s); consequently, they are able to present similar reaction behavior as observed in solution-phase photooxidation. In particular: (1) a single water molecule is sufficient to stabilize the hydroperoxide product; (2) conformers with water bound at different sites may follow different reaction pathways. For example, hydrated CysH$^+$ with water bound to the ammonium group shows water-assisted proton transfer; (3) addition of the second water molecules significantly enhances the reaction efficiency of CysH$^+$, but has little effect on that of deprotonated Cys;

(4) in spite of the resemblances between the reaction mechanisms of hydrated protonated and deprotonated Cys (as both show complex-mediation and formation of persulfoxide/hydroperoxide followed by elimination of water), hydrated $CysH^+$ shows much higher efficiencies in forming hydroperoxides with $^1O_2$ than hydrated deprotonated Cys, mimicking the pH dependence observed in solution-phase photooxidation of Cys.[25]

Acknowledgements

This work was supported by the National Science Foundation CAREER Award (#CHE-0954507), Queens College Research Enhancement Funds, and PSC-CUNY Research Awards. We thank Yigang Fang for his assistance with LabVIEW programming for mass spectrometry experiments, and Alec Greer (CUNY Brooklyn) for his valuable comments on the manuscript.

References

1 M. J. Davies, *Biochem. Biophys. Res. Commun.*, 2003, **305**, 761–770.
2 M. J. Davies, *Biochim. Biophys. Acta*, 2005, **1703**, 93–109.
3 G. Palumbo, *Expert Opin. Drug Delivery*, 2007, **4**, 131–148.
4 K. G. McGregor and C. Anastasio, *Atmos. Environ.*, 2001, **35**, 1091–1104.
5 C. S. Foote, *Science*, 1968, **162**, 963–970.
6 C. Schweitzer and R. Schmidt, *Chem. Rev.*, 2003, **103**, 1685–1757.
7 Y. Fang and J. Liu, *J. Phys. Chem. A*, 2009, **113**, 11250–11261.
8 Y. Fang, F. Liu, A. Bennett, S. Ara and J. Liu, *J. Phys. Chem. B*, 2011, **115**, 2671–2682.
9 F. Liu, Y. Fang, Y. Chen and J. Liu, *J. Phys. Chem. B*, 2011, **115**, 9898–9909.
10 F. Liu, Y. Fang, Y. Chen and J. Liu, *J. Phys. Chem. B*, 2012, **116**, 6369–6379.
11 Y. Fang, F. liu, R. Emre and J. Liu, *J. Phys. Chem. B*, 2013, **117**, 2878–2887.
12 M. Yamashita and J. B. Fenn, *J. Phys. Chem.*, 1984, **88**, 4451–4459.
13 J. B. Fenn, M. Mann, C. K. Meng, S. F. Wong and C. M. Whitehouse, *Science*, 1989, **246**, 64–71.
14 D. Gerlich, in *State-Selected and State-to-State Ion-Molecule Reaction Dynamics. Part I. Experiment*, ed. C. Y. Ng and M. Baer, John Wiley & Sons, Inc., New York, 1992, vol. 82, pp. 1–176.
15 D. Liu, T. Wyttenbach and M. T. Bowers, *Int. J. Mass Spectrom.*, 2004, **236**, 81–90.
16 P. H. Fishman, J. W. Kusiak and J. M. Bailey, *Biochem.*, 1973, **12**, 2540–2544.
17 G. Gennari, G. Cauzzo and G. Jori, *Photochem. Photobiol.*, 1974, **20**, 497–500.
18 S. Cannistraro, G. Jori and A. van der Vorst, *Photochem. Photobiol.*, 1978, **27**, 517–521.
19 R. C. Straight and J. D. Spikes, in *Singlet O_2, Vol. 4: Polymers and Biomolecules*, ed. A. A. Frimer, CRC Press, Boca Raton, Florida, 1985, pp. 91–143.
20 W. Ando and T. Takata, in *Singlet O_2,Vol. 3: Reaction Modes and Products Part 2*, ed. A. A. Frimer, CRC Press, Boca Raton, 1985, pp. 1–117.
21 M. Rougee, R. V. Bensasson, E. J. Land and R. Pariente, *Photochem. Photobiol.*, 1988, **47**, 485–489.
22 G. Z. Justo, F. A. Camargo, M. Haun, A. Faljoni-Alario and N. Duran, *Physiol. Chem. Phys. Med. NMR*, 2000, **32**, 145–154.
23 M. J. Davies, *Photochem. Photobiol. Sci.*, 2004, **3**, 17–25.
24 E. L. Clennan, *Acc. Chem. Res.*, 2001, **34**, 875–884.
25 A. A. Frimer, *Singlet O_2, Vol III, Reaction Modes and Products, Part 2,* CRC Press, Boca Raton, FL, 1985.
26 H. Wincel, *Int. J. Mass Spectrom.*, 2006, **251**, 23–31.
27 Y. Fang, A. Bennett and J. Liu, *Int. J. Mass Spectrom.*, 2010, **293**, 12–22.
28 Y. Fang, A. Bennett and J. Liu, *Phys. Chem. Chem. Phys.*, 2011, **13**, 1466–1478.
29 S. E. Rodriguez-Cruz, J. S. Klassen and E. R. Williams, *J. Am. Soc. Mass Spectrom.*, 1997, **8**, 565–568.
30 R. M. Moision and P. B. Armentrout, *J. Am. Soc. Mass Spectrom.*, 2007, **18**, 1124–1134.
31 A. N. Krutchinsky, I. V. Chernushevich, V. L. Spicer, W. Ens and K. G. Standing, *J. Am. Soc. Mass Spectrom.*, 1998, **9**, 569–579.
32 K. M. Ervin and P. B. Armentrout, *J. Chem. Phys.*, 1985, **83**, 166–189.
33 P. B. Armentrout, *J. Anal. At. Spectrom.*, 2004, **19**, 571–580.
34 A. Midey, I. Dotan and A. A. Viggiano, *J. Phys. Chem. A*, 2008, **112**, 3040–3045.
35 A. J. Midey, I. Dotan and A. A. Viggiano, *Int. J. Mass Spectrom.*, 2008, **273**, 7–10.
36 W. J. Lafferty, A. M. Solodov, C. L. Lugez and G. T. Fraser, *Appl. Opt.*, 1998, **37**, 2264–2270.
37 J. Troe, *Chem. Phys. Lett.*, 1985, **122**, 425–430.
38 M. J. Frisch, G. W. Trucks, H. B. Schlegel, G. E. Scuseria, M. A. Robb, J. R. Cheeseman, G. Scalmani, V. Barone, B. Mennucci, G. A. Petersson, H. Nakatsuji, M. Caricato, X. Li, H. P. Hratchian, A. F. Izmaylov, J. Bloino, G. Zheng, J. L. Sonnenberg, M. Hada, M. Ehara, K. Toyota, R. Fukuda, J. Hasegawa, M. Ishida, T. Nakajima, Y. Honda, O. Kitao, H. Nakai, T. Vreven, J. J. A. Montgomery, J. E. Peralta, F. Ogliaro, M. Bearpark, J. J. Heyd, E. Brothers, K. N. Kudin, V. N. Staroverov, T. Keith, R. Kobayashi, J. Normand, K. Raghavachari, A. Rendell, J. C. Burant, S. S. Iyengar, J. Tomasi, M. Cossi, N. Rega, J. M. Millam, M. Klene, J. E. Knox, J. B. Cross, V. Bakken, C. Adamo, J. Jaramillo, R. Gomperts, R. E. Stratmann, O. Yazyev, A. J. Austin, R. Cammi, C. Pomelli, J. W. Ochterski, R. L. Martin, K. Morokuma, V. G. Zakrzewski, G. A. Voth, P. Salvador, J. J. Dannenberg, S. Dapprich, A. D. Daniels, O. Farkas, J. B. Foresman, J. V. Ortiz, J. Cioslowski and D. J. Fox, *Gaussian 09, Rev. B. 01*, Gaussian, Inc., Wallingford, CT, 2009.
39 J. Zheng, I. M. Alecu, B. J. Lynch, Y. Zhao and D. G. Truhlar, Database of Frequency Scale Factors for Electronic Model Chemistries, Version 2, http://comp.chem.umn.edu/freqscale/version2.htm, 2010.

40 W. L. Hase, K. Song and M. S. Gordon, *Comput. Sci. Eng.*, 2003, **5**, 36–44.
41 W. L. Hase, K. Bolton, P. de Sainte Claire, R. J. Duchovic, X. Hu, A. Komornicki, G. Li, K. Lim, D. Lu, G. H. Peslherbe, K. Song, K. N. Swamy, S. R. Vande Linde, A. Varandas, H. Wang and R. J. Wolf, *VENUS 99: A general chemical dynamics computer program*, Texas Tech Univeristy Lubbock, TX, 1999.
42 V. Bakken, J. M. Millam and H. B. Schlegel, *J. Chem. Phys.*, 1999, **111**, 8773–8777.
43 G. B. Bacskay, *Chem. Phys.*, 1981, **61**, 385–404.
44 L. Laaksonen, gOpenMol, Center for Scientific Computing, Espoo, Finland, 3.0 ed., 2005, available at www.csc.fi/gopenmol/.
45 Y. Yao, D. Chen, S. Zhang, Y. Li, P. Tu, B. Liu and M. Dong, *J. Phys. Chem. B*, 2011, **115**, 6213–6221.
46 C. Michaux, J. Wouters, E. A. Perpète and D. Jacquemin, *J. Am. Soc. Mass Spectrom.*, 2009, **20**, 632–638.
47 M. Rozman, *J. Am. Soc. Mass Spectrom.*, 2005, **16**, 1846–1852.
48 B. Gao, T. Wyttenbach and M. T. Bower, *J. Am. Chem. Soc.*, 2009, **131**, 4695–4701.
49 H. Wincel, *Chem. Phys. Lett.*, 2007, **439**, 157–161.
50 P. Vollhardt and N. Schore, *Organic Chemistry*, W. H. Freeman and Company, New York, 2009.
51 H.-K. Woo, K.-C. Lau, X.-B. Wang and L.-S. Wang, *J. Phys. Chem. A*, 2006, **110**, 12603–12606.
52 Z. Tian, A. Pawlow, J. C. Poutsma and S. R. Kass, *J. Am. Chem. Soc.*, 2007, **129**, 5403–5407.
53 J. Oomens, J. D. Steill and B. Redlich, *J. Am. Chem. Soc.*, 2009, **131**, 4310–4319.
54 Z. Tian and S. R. Kass, *J. Am. Chem. Soc.*, 2008, **130**, 10842–10843.
55 Z. Tian, X.-B. Wang, L.-S. Wang and S. R. Kass, *J. Am. Chem. Soc.*, 2009, **131**, 1174–1181.
56 D. Liu, T. Wyttenbach, C. J. Carpenter and M. T. Bowers, *J. Am. Chem. Soc.*, 2004, **124**, 3261–3270.
57 H. Wincel, *J. Am. Soc. Mass Spectrom.*, 2008, **19**, 1091–1097.
58 T. Wyttenbach, D. Liu and M. T. Bowers, *Int. J. Mass Spectrom.*, 2005, **240**, 221–232.
59 K. M. Ervin, I. Anusiewicz, P. Skurski, J. Simons and W. C. Lineberger, *J. Phys. Chem. A*, 2003, **107**, 8521–8529.
60 J. M. Matxain, M. Ristilae, A. Strid and L. A. Eriksson, *Chem.–Eur. J.*, 2007, **13**, 4636–4642.
61 A. A. Viggiano, A. Midey, N. Eyet, V. M. Bierbaum and J. Troe, *J. Chem. Phys.*, 2009, **131**, 094303.
62 F. Wilkinson, W. P. Helman and A. B. Ross, *J. Phys. Chem. Ref. Data*, 1995, **24**, 663–1021.
63 M. B. Knickelbein and W. B. Menezes, *Phys. Rev. Lett.*, 1992, **69**, 1046–1049.
64 W. J. C. Menezes and M. B. Knickelbein, *J. Chem. Phys.*, 1993, **98**, 1856–1866.
65 G. Gregoire and M. A. Duncan, *J. Chem. Phys.*, 2002, **117**, 2120–2130.
66 J. H. Jensen and M. S. Gordon, *J. Am. Chem. Soc.*, 1995, **117**, 8159–8170.